Abstracta

Ano XVIII - N. 06

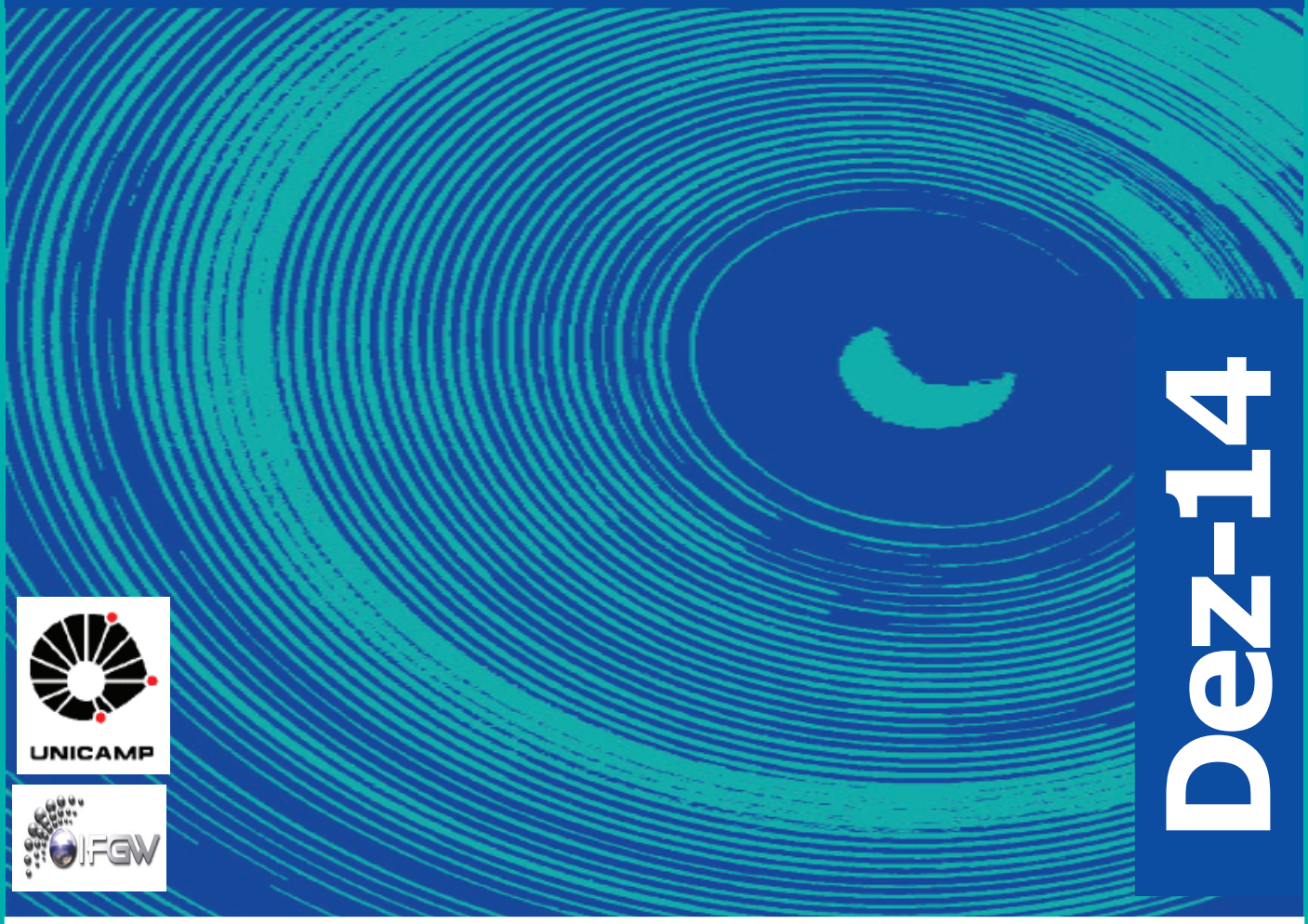

Dez-14

UNICAMP

IFGW

Trabalhos Publicados - P321-2014 à P354-2014

Trabalhos Aceitos para Publicação - A001-2014 à A002-2014

Correção - C077-2014

Defesas de Dissertações do IFGW - D016-2014 à D017-2014

Defesas de Teses do IFGW - T026-2014 à T027-2014

Trabalhos Publicados

[P321-2014] "alpha B-crystallin interacts with and prevents stress-activated proteolysis of focal adhesion kinase by calpain in cardiomyocytes"

Pereira, M. B. M.; Santos, A. M.; Goncalves, D. C.; Cardoso, A. C.; Consonni, S. R.; Gozzo, F. C.; Oliveira, P. S.; Pereira, A. H. M.; Figueiredo, A. R.; Tiroli-Cepeda, A. O.; Ramos, C. H. I.; **de Thomaz, A. A.*; Cesar, C. L.***; Franchini, K. G.

Focal adhesion kinase (FAK) contributes to cellular homeostasis under stress conditions. Here we show that alpha B-crystallin interacts with and confers protection to FAK against calpain--mediated proteolysis in cardiomyocytes. A hydrophobic patch mapped between helices 1 and 4 of the FAK FAT domain was found to bind to the beta 4-beta 8 groove of alpha B-crystallin. Such an interaction requires FAK tyrosine 925 and is enhanced following its phosphorylation by Src, which occurs upon FAK stimulation. alpha B-crystallin silencing results in calpain-dependent FAK depletion and in the increased apoptosis of cardiomyocytes in response to mechanical stress. FAK overexpression protects cardiomyocytes depleted of alpha B-crystallin against the stretch-induced apoptosis. Consistently, load-induced apoptosis is blunted in the hearts from cardiac-specific FAK transgenic mice transiently depleted of alpha B-crystallin by RNA interference. These studies define a role for alpha B-crystallin in controlling FAK function and cardiomyocyte survival through the prevention of calpain-mediated degradation of FAK.

Nature Communications 5, 5159, 2014. DOI: 10.1038/ncomms6159

[P322-2014] "Analysis of immersed silica optical microfiber knot resonator and its application as a moisture sensor"

Gouveia, M. A.*; Pellegrini, P. E. S.*; dos Santos, J. S.; Raimundo, I. M.; **Cordeiro, C. M. B.***

An embedded silica optical microfiber knot resonator humidity sensor is presented. As silica has a poor response to environmental humidity changes, a surrounding layer of Nafion is used as a transducer. Spectral characterization and also a procedure to determine the coupling and total loss coefficients are presented. Sensitivity as high as (0.29 +/- 0.01) nm/% relative humidity has been noticed. Possible issues that emerge from the use of Nafion such as bulk swelling, refractive index hysteresis, as well as a saturation process, are discussed.

Applied Optics 53[31], 7454-7461, 2014. DOI: 10.1364/AO.53.007454

[P323-2014] "Au and Pd nanoparticles supported on CeO2, TiO2, and Mn2O3 oxides"

Nascente, P. A. P.; Maluf, S. S.; Afonso, C. R. M.; **Landers, R.*;** Pinheiro, A. N.; Leite, E. R.

Gold and palladium nanoparticles were incorporated on CeO2, TiO2 , and Mn2O3 supports prepared by a sol-gel method. The samples were characterized by X-ray diffraction (XRD), X-ray photoelectron spectroscopy (XPS), energy dispersive spectroscopy (EDS), transmission electron microscopy (TEM), high resolution TEM (HRTEM), scanning TEM (STEM) in high angle annular dark field mode (HAADF), and energy filtered TEM (EFTEM) using electron energy loss spectroscopy (EELS). The XRD diffractograms presented sharp and intense peaks indicating that the samples are highly crystalline, but it did not detected any peak corresponding to Au or Pd phases. This indicates that the Au and Pd NPs were incorporated into the structures of the oxides. It was not possible to obtain an Au 4f spectrum for Au/Mn2O3 due to an overlap with the Mn 3p spectrum. The XPS Au 4f spectra for Au/CeO2 and Au/TiO2 present negative chemical shifts that could be attributed to particle-size-related properties. The XPS Pd 3d spectra indicate that for both CeO2 and TiO2 substrates, the Pd NPs were in the metallic state, while for the Mn2O3 substrate, the Pd NPs were oxidized. The HRTEM results show the formation of nanocrystalline oxides having particles sizes between 50 and 200 nm. TEM micrographs show that the addition of Au caused the formation of Au clusters in between the CeO2 NPS, formation of Au NPs for the TiO2 support, and homogeneous distribution of Au clusters for the Mn2O3 support. The addition of Pd yielded a homogeneous dispersion throughout the CeO2 and TiO2, but caused the formation of Pd clusters for the Mn2O3 support.

Applied Surface Science 315, 490-498, 2014. DOI: 10.1016/j.apsusc.2014.04.090

[P324-2014] "Compact Ag@Fe3O4 Core-shell Nanoparticles by Means of Single-step Thermal Decomposition Reaction"

Brollo, M. E. F.*; Lopez-Ruiz, R.*; Muraca, D.*; Figueroa, S. J. A.; **Pirota, K. R.*; Knobel, M.***

A temperature pause introduced in a simple single-step thermal decomposition of iron, with the presence of silver seeds formed in the same reaction mixture, gives rise to novel compact heterostructures: brick-like Ag@Fe3O4 core-shell nanoparticles. This novel method is relatively easy to implement, and could contribute to overcome the challenge of obtaining a multifunctional heteroparticle in which a noble metal is surrounded by magnetite. Structural analyses of the samples show 4 nm silver nanoparticles wrapped within compact cubic external structures of Fe oxide, with curious rectangular shape. The magnetic properties indicate a near superparamagnetic like behavior with a weak hysteresis at room temperature. The value of the anisotropy involved makes these particles candidates to potential applications in nanomedicine.

Scientific Reports 4, 6839, 2014. DOI: 10.1038/srep06839

[P325-2014] "Discrete trinuclear copper(II) compounds as building blocks: the influence of the peripheral substituents on the magnetic coupling in oxamato-bridged complexes"

Barros, W. P.; da Silva, B. C.; Reis, N. V.; Pereira, C. L. M.; Doriguetto, A. C.; Cano, J.; **Pirota, K. R.***; Pedroso, E. F.; Julve, M.; Stumpf, H. O.

Two new trinuclear copper(II) complexes without end-capping ligands, (Bu4N)(2)[Cu(dmso)(2){Cu(dnopba)(dmso)}(2)] (1) and (Bu4N)(2)[Cu(dmso)(2){Cu(dcopba)(dmso)}(2)] (2) [dnopba = 4,5-dinitro-ortho-phenylenebis(oxamate), dcopba = 4,5-dichloro-ortho-phenylenebis(oxamate), Bu4N+ = tetra-n--butylammonium and dmso = dimethylsulfoxide], were synthesized and their structures were determined by single crystal X-ray diffraction. The crystal structures of 1 and 2 consist of two outer bis(oxamato)(dmso)cuprate(II) units which act as bidentate ligands toward a trans-bis(dmso)copper(II) inner entity leading to centrosymmetric tricopper(II) complexes with copper-copper separations across the oxamate bridges of 5.1916(3) (1) and 5.1776(3) angstrom (2). The peripheral copper(II) ions in 1 and 2 are five-coordinate in somewhat distorted square pyramidal environments with a dmso molecule fitting the apical position whereas the inner copper(II) ion is six-coordinate in an elongated octahedral environment with two dmso molecules in the axial sites. The investigation of their magnetic properties in the temperature range 2.0-300 K shows the occurrence of a strong intramolecular antiferromagnetic coupling between the copper(II) ions through the oxamate bridges [J(1) = -296(1) (1) and -334(1) cm(-1) (2),

the Hamiltonian being defined as (H) over cap = -J(1)((S) over cap (Cu2)center dot(S) over cap (Cu1) + (S) over cap (Cu2)center dot(S) over cap (Cu1)center dot)], which leads to a low-lying spin doublet at low temperatures. Density functional theory calculations (DFT) have been used to substantiate these magnetic couplings and also to analyse the influence exerted on these interactions by the type of substituent at the 4,5-positions from the phenylene ring of the bis(oxamate) ligand.

Dalton Transactions 43[39], 14586-14595, 2014. DOI: 10.1039/c4dt01180e

[P326-2014] "Distinct functional and structural MRI abnormalities in mesial temporal lobe epilepsy with and without hippocampal sclerosis"

Coan, A. C.; Campos, B. M.; **Beltramini, G. C.*;** Yasuda, C. L.; **Covolan, R. J. M.*; Cendes, F.**

Objective: We aimed to investigate patterns of electroencephalography-correlated functional MRI (EEG-fMRI) and subtle structural abnormalities in patients with mesial temporal lobe epilepsy (MTLE) with hippocampal sclerosis (MTLE-HS) or normal MRI (MTLE-NL). Methods: We evaluated EEG-fMRI acquisition of the 25 patients with diagnosis of MTLE who had interictal epileptiform discharges (IEDs) in the intra-MRI EEG: 13 MTLE-HS and 12 MTLE-NL. fMRI was performed using echo-planar images in a 3T MRI coupled with EEG acquired with 64 MRI-compatible electrodes. In the first level analyses, the time of the IEDs ipsilateral to the epileptogenic zone was used as the paradigm, and four contrasts maps were built according to the variation of the hemodynamic response function (HRF) peaks (0, + 3, + 5, and + 7 s). Second level group analyses were performed combining the contrast maps of MTLE-HS or MTLE-NL patients with each different HRF obtained at the first level. Areas of gray matter atrophy were evaluated with voxel-based morphometry (VBM) in both groups. Results: MTLE-HS and MTLE-NL had IED-related positive BOLD (posBOLD) detected in the ipsilateral anterior temporal lobe and insula. However, only MTLE-HS had significant posBOLD on contralateral hippocampus and anterior cingulate, whereas MTLE-NL had areas of posBOLD on ipsilateral frontal lobe. Both groups had significant IED-related negBOLD responses in areas of the default mode network (DMN), such as posterior cingulate and precuneus. There was no overlap of both posBOLD and negBOLD and areas of atrophy detected by VBM. Significance: Similar IEDs have different patterns of hemodynamic responses in subgroups of MTLE. In both MTLE-HS and MTLE-NL, there is a possible suppression of the DMN related to IEDs, as demonstrated by the negBOLD in these areas. The brain areas involved in the interictal related hemodynamic network are not the regions with the most significant gray matter atrophy in MTLE with or without MRI signs of HS.

Epilepsia 55[8], 1187-1196, 2014. DOI: 10.1111/epi.12670

[P327-2014] "Efficient finite-time measurements under thermal regimes"

Brasil, C. A.*; de Castro, L. A.; Napolitano, R. D.

Contrary to conventional quantum mechanics, which treats measurement as instantaneous, here we explore a model for finite-time measurement. The main two-level system interacts with the measurement apparatus in a Markovian way described by the Lindblad equation, and with an environment, which does not include the measuring apparatus. To analyse the environmental effects on the final density operator, we use the Redfield approach, allowing us to consider a non-Markovian noise. In the present hybrid theory, to trace out the environmental degrees of freedom, we use a previously developed analytic method based on superoperator algebra and Nakajima-Zwanzig superoperators. Here, we analyse two types of system-environment interaction, phase and amplitude damping, which allows us to conclude that, in general, a finite-time quantum measurement performed during a certain period is more efficient than an instantaneous measurement performed at the end of it, because the rate of change of the populations is attenuated by the system-measurement apparatus interaction.

European Physical Journal Plus 129[10], 206, 2014. DOI: 10.1140/epjp/i2014-14206-0

[P328-2014] "Experimental Realization of TiO2 Nanosponge/Spin-coated P3HT Heterojunction Solar Cells"

Thomazi, F.; de Souza, M. R.; Saul, C. K.; **Viana, G. A.*; Marques, F. C.*;** Silvestre, R. G. M.; Brehm, M. A.; Marino, C. E. B.; Burkarter, E.; Dartora, C. A.

Production and characterization of multilayered polymer solar cells consisting of P3HT thin films deposited on titanium dioxide nanosponges are reported. The photovoltaic response is remarkable, considering the simplicity of the thin film production method employed here. The nanostructured TiO2 anodic films were grown in buffered aqueous phosphoric acid solutions under potentiostatic regime at room temperature and then characterized using scanning electron microscopy. The P3HT films were prepared by spin coating technique and the samples were annealed at 180 degrees C. Conversion efficiencies around 0.4% were obtained, with open circuit voltages and short circuit current densities as high as 560 mV and 2.7 mA/cm(2), respectively.

Current Nanoscience 10[6], 877-882, 2014.

[P329-2014] "Flow harmonics within an analytically solvable viscous hydrodynamic model"

Hatta, Y.; Noronha, J.; **Torrieri, G.*;** Xiao, B. W.

Based on a viscous hydrodynamic model with anisotropically perturbed Gubser flow and isothermal Cooper-Frye freeze-out at early times, we analytically compute the flow harmonics nu(n)(p(T)) and study how they scale with the harmonic number n and transverse momentum, as well as the system size, shear, and bulk viscosity coefficients, and collision energy. In particular, we find that the magnitude of shear viscous corrections grows linearly with n. The mixing between different harmonics is also discussed. While this model is rather simple as compared to realistic heavy-ion collisions, we argue that the scaling results presented here may be meaningfully compared to experimental data collected over many energies, system sizes, and geometries.

Physical Review D 90[7], 074026, 2014. DOI: 10.1103/PhysRevD.90.074026

[P330-2014] "Improved measurements of the neutrino mixing angle theta(13) with the Double Chooz detector"

Abe, Y.; dos Anjos, J. C.; Barriere, J. C.; **Gonzalez, L. F. G.*; Kemp, E.*;** et al.
Double Chooz Collaboration

The Double Chooz experiment presents improved measurements of the neutrino mixing angle theta(13) using the data collected in 467.90 live days from a detector positioned at an average distance of 1050m from two reactor cores at the Chooz nuclear power plant.

Several novel techniques have been developed to achieve significant reductions of the backgrounds and systematic uncertainties with respect to previous publications, whereas the efficiency of the (nu) over bar (e) signal has increased. The value of theta(13) is measured to be sin(2)2 theta(13) = 0.090(-0.029)(+0.032) from a fit to the observed energy spectrum. Deviations from the reactor (nu) over bar (e) prediction observed above a prompt signal energy of 4 MeV and possible explanations are also reported. A consistent value of theta(13) is obtained from a fit to the observed rate as a function of the reactor power independently of the spectrum shape and background estimation, demonstrating the robustness of the theta(13) measurement despite the observed distortion.

Journal Of High Energy Physics [10], 086, 2014. DOI: 10.1007/JHEP10(2014)086

[P331-2014] "Influence of the chemical surface structure on the nanoscale friction in plasma nitrided and post-oxidized ferrous alloy"

Freislebem, M.; Menezes, C. M.; Cemin, F.; Costi, F. B.; Ferreira, P. A.; Aguzzoli, C.; Baumvol, I. J. R.; **Alvarez, F.*;** Figueroa, C. A.

Friction is a ubiquitous phenomenon in everyday activities spanning from vehicles where efficient brakes are mandatory up to mechanical devices where its minimum effects are pursued for energy efficiency issues. Recently, theoretical models succeed correlating the friction behavior with energy transference via phonons between sliding surfaces. Therefore, considering that the energy losses by friction are prompted through phonons, the chemical surface structure between sliding surfaces is very important to determine the friction phenomenon. In this work, we address the issue of friction between a conical diamond tip sliding on different functionalized flat steel surfaces by focusing the influence of the chemical bonds in the outermost layers on the sliding resistance. This geometry allows probing the coupling of the sharp tip with terminator species on the top and underneath material surface at in-depth friction measurements from 20 to 200 nm. Experimentally, the friction coefficient decreases when nitrogen atoms are substituted for oxygen in the iron network. This effect is interpreted as due to energy losses through phonons whilst lower vibrational frequency excitation modes imply lower friction coefficients and a more accurate adjustment is obtained when a theoretical model with longitudinal adsorbate vibration is used.

Applied Physics Letters 105[11], 111603, 2014. DOI: 10.1063/1.4894803

[P332-2014] "Inorganic Graphenylene: A Porous Two-Dimensional Material With Tunable Band Gap"

Perim, E.*; Paupitz, R.; **Autreto, P. A. S.*; Galvao, D. S.***

By means of ab initio calculations, we investigate the possibility of existence of a boron nitride (BN) porous two-dimensional nanosheet, which is geometrically similar to the carbon allotrope known as biphenylene carbon. The proposed structure, which we called inorganic graphenylene (IGP), is formed spontaneously after selective dehydrogenation of the porous boron nitride (BN) structure proposed by Ding et al. We study the structural and electronic properties of both porous BN and IGP, and it is shown that, by selective substitution of B and N atoms with carbon atoms in these structures, the band gap can be significantly reduced, changing their behavior from insulators to semiconductors, thus opening the possibility of band gap engineering for this class of two-dimensional materials.

Journal Of Physical Chemistry C 118[41], 23670-23674, 2014. DOI: 10.1021/jp502119y

[P333-2014] "Line intensity measurements of methane's -band using a cw-OPO"

Moreno, M. P.; Cadoret, M.; Jahjah, M.; Nguyen, L.; **Cruz, F. C.*;** Zondy, J. J.

We report on absolute line strength measurements of P(1), R(0) and R(1) singlet lines in the (C-H stretching) band of methane at reference temperature K. Line strength measurements are performed at low pressure using direct absorption spectroscopy technique based on a widely tunable continuous-wave singly resonant optical parametric oscillator. The overall accuracy in line strength determinations ranges between 7 and 8 % mostly limited by pressure and frequency measurements. A comparison with previous reported values is made. Our results show good agreement with the HITRAN 2012 database.

Applied Physics B-Lasers And Optics 117[2], 681-687, 2014. DOI: 10.1007/s00340-014-5883-1

[P334-2014] "Magnetic and structural investigations on La0.6Sr0.4MnO3 nanostructured manganite: Evidence of a ferrimagnetic shell"

Andrade, V. M.; Caraballo-Vivas, R. J.; Costas-Soares, T.; Pedro, S. S.; Rocco, D. L.; Reis, M. S.; Campos, A. P. C.; **Coelho, A. A.***

This paper presents the structural and magnetic properties of La0.6Sr0.4MnO3 nanoparticles with sizes from 21 to 106 nm, which have been prepared using the sol-gel method. The reduction of the nanoparticles' size tends to broaden the paramagnetic to ferromagnetic transition, as well as to promote magnetic hysteresis and a remarkable change on the magnetic saturation. In order to better understand the magnetic behavior of those nanoparticles, a simple model based on a ferromagnetic core and a ferrimagnetic shell was considered, where the magnetization was described in terms of the standard mean-field Brillouin function. This model matches the experimental data, leading to conclusion the nanoparticles with size <40 nm are single magnetic domain. In addition, the output fitting parameters give information on the Lande factor of the core and shell.

Journal Of Solid State Chemistry 219, 87-92, 2014. DOI: 10.1016/j.jssc.2014.07.013

[P335-2014] "Magnetic moment of Fe3O4 films with thicknesses near the unit-cell size"

Gomes, G. F. M.; Bueno, T. E. P.; Parreiras, D. E.; **Abreu, G. J. P.*; de Siervo, A.*;** Cezar, J. C.; Pfannes, H. D.; Paniago, R.

We perform a systematic study on the evolution of the magnetic spin moment (m(s)) of epitaxial [100]- and [111]-magnetite films of increasing thickness. The ultrathin films are characterized by low-energy electron diffraction, x-ray absorption spectroscopy, and x-ray magnetic circular dichroism (XMCD). By employing sum rules on the XMCD spectra we obtain m(s) = 3.6 mu(B)/f.u. for samples of around 35 angstrom. This is considered a bulk value and has been reported only for films more than 10 times thicker. Moreover, we show that even 10-angstrom-thick magnetite already presents a significant magnetic moment. For both grown directions the moment increases similarly with the thickness. The ferromagnetic behavior for each iron ion site (Fe-octa(2+), Fe-octa(3+), Fe--tetra(3+)) of Fe3O4 is measured by monitoring XMCD peaks. The deduced hysteresis curves (per ion, per site) exhibit a coercive field of 300 Oe. Our results show that both the ferrimagnetic order and the bulk moment value are preserved at room temperature around the thickness of 2 unit cells.

Physical Review B 90[13], 134422, 2014. DOI: 10.1103/PhysRevB.90.134422

[P336-2014] "Measurement of prompt J/psi pair production in pp collisions at root s = 7 Tev"

Khachatryan, V.; Sirunyan, A. M.; Tumasyan, A.; **Chinellato, J.*; Tonelli Manganote, E. J.*;** et al.
CMS Collaboration

Production of prompt J/psi meson pairs in proton-proton collisions at root s = 7 TeV is measured with the CMS experiment at the LHC in a data sample corresponding to an integrated luminosity of about 4.7 fb(-1). The two J/psi mesons are fully reconstructed via their decays into mu(+)mu(-) pairs. This observation provides for the first time access to the high-transverse-momentum region of J/psi pair production where model predictions are not yet established. The total and differential cross sections are measured in a phase space defined by the individual J/psi transverse momentum (p(T)(J/psi)) and rapidity (vertical bar y(J/psi)vertical bar): vertical bar y(J/psi)vertical bar < 1.2 for p(T)(J/psi) > 6.5 GeV/c; 1.2 < vertical bar y(J/psi)vertical bar < 1.43 for a pT threshold that scales linearly with vertical bar y(J/psi)vertical bar from 6.5 to 4.5 GeV/c; and 1.43 < vertical bar y(J/psi)vertical bar < 2.2 for p(T)(J/psi) > 4.5 GeV/c. The total cross section, assuming unpolarized prompt J/psi pair production is 1.49 +/- 0.07 (stat) +/- 0.13 (syst) nb. Different assumptions about the J/psi polarization imply modifications to the cross section ranging from -31% to +27%.

Journal Of High Energy Physics [9], 094, 2014. DOI: 10.1007/JHEP09(2014)094

[P337-2014] "Measurement of the ratio of inclusive jet cross sections using the anti-k(T) algorithm with radius parameters R=0.5 and 0.7 in pp collisions at root s=7 TeV"

Chatrchyan, S.; Khachatryan,V.; Sirunyan, A. M.; **Chinellato, J.*; Manganote, E. J. Tonelli***; et al.
CMS Collaboration

Measurements of the inclusive jet cross section with the anti-k(T) clustering algorithm are presented for two radius parameters, R = 0.5 and 0.7. They are based on data from LHC proton-proton collisions at root s = 7 TeV corresponding to an integrated luminosity of 5.0 fb(-1) collected with the CMS detector in 2011. The ratio of these two measurements is obtained as a function of the rapidity and transverse momentum of the jets. Significant discrepancies are found comparing the data to leading-order simulations and to fixed-order calculations at next-to-leading order, corrected for nonperturbative effects, whereas simulations with next-to-leading-order matrix elements matched to parton showers describe the data best.

Physical Review D 90[7], 072006, 2014. DOI: 10.1103/PhysRevD.90.072006

[P338-2014] "Observation of D-0 Meson Nuclear Modifications in Au plus Au Collisions at root(NN)-N-s=200 GeV"

Adamczyk, L.; Adkins, J. K.; Agakishiev, G.; **Derradi de Souza, R.*; Takahashi, J.*; Vasconcelos, G. M. S.*;** et al.
STAR Collaboration

We report the first measurement of charmed-hadron (D-0) production via the hadronic decay channel (D-0 -> K- + pi(+)) in Au + Au collisions at root(NN)-N-s = 200 GeV with the STAR experiment. The charm production cross section per nucleon- nucleon collision at midrapidity scales with the number of binary collisions, N-bin, from p + p to central Au + Au collisions. The D-0 meson yields in central Au + Au collisions are strongly suppressed compared to those in p + p scaled by N-bin, for transverse momenta p(T) > 3 GeV/c, demonstrating significant energy loss of charm quarks in the hot and dense medium. An enhancement at intermediate p(T) is also observed. Model calculations including strong charm-medium interactions and coalescence hadronization describe our measurements.

Physical Review Letters 113[14], 142301, 2014. DOI: 10.1103/PhysRevLett.113.142301

[P339-2014] "On the hydrogenated silicon carbide (SiCx:H) interlayer properties prompting adhesion of hydrogenated amorphous carbon (a-C:H) deposited on steel"

Cemin, F.; Bim, L. T.; Menezes, C. M.; Aguzzoli, C.; da Costa, M. E. H.; Baumvol, I. J. R.; **Alvarez, F.***; Figueroa, C. A.

This work reports a systematic study of physical chemical properties of SiCx:H interlayers deposited by using tetramethylsilane on AISI 4140 at different temperatures (100 degrees C-550 degrees C) and its effects on the adhesion of a-C:H thin films. The bi-layers were obtained by pulsed-DC PECVD assisted by electrostatic confinement. The results show that the thickness of the SiCx:H interlayer exponentially decreases as the deposition temperature increases, i.e., a thermally activated kinetic process controls the global chemical reaction in the interlayer. There is a transition temperature (similar to 300 degrees C) for interlayer deposition where adhesion of a-C:H is reached. Above similar to 300 degrees C, the a-C:H thin films show critical loads to wedge spallation from 298 (300 degrees C) to 478 mN (550 degrees C). At higher temperatures, H and Si contents decrease whereas C content increases in the interlayer. The improved adhesion is associated with the nature of chemical bonds formed in the interlayer.

VACUUM 109[SI], 180-183, 2014. DOI: 10.1016/j.vacuum.2014.07.015

[P340-2014] "One-dimensional silicon and germanium nanostructures with no carbon analogues"

Perim, E.*; Paupitz, R.; Botari, T.; **Galvao, D. S.***

In this work we report new silicon and germanium tubular nanostructures with no corresponding stable carbon analogues. The electronic and mechanical properties of these new tubes were investigated through ab initio methods. Our results show that these structures have lower energy than their corresponding nanoribbon structures and are stable up to high temperatures (500 and 1000 K, for silicon and germanium tubes, respectively). Both tubes are semiconducting with small indirect band gaps, which can be significantly altered by both compressive and tensile strains. Large band-gap variations of almost 50% were observed for strain rates as small as 3%, suggesting their possible applications in sensor devices. They also present high Young's modulus values (0.25 and 0.15 TPa, respectively). TEM images were simulated to help in the identification of these new structures.

Physical Chemistry Chemical Physics 16[44], 24570-24574, 2014. DOI: 10.1039/c4cp03708a

[P341-2014] "Ortho-positronium observation in the Double Chooz experiment"

Abe, Y.; dos Anjos, J. C.; Barriere, J. C.; **Gonzalez, L. F. G.*; Kemp, E.*;** et al.
Double Chooz Collaboration

The Double Chooz experiment measures the neutrino mixing angle theta(13) by detecting reactor (nu) over bar (e) via inverse beta decay. The positron-neutron space and time coincidence allows for

a sizable background rejection, nonetheless liquid scintillator detectors would profit from a positron/electron discrimination, if feasible in large detector, to suppress the remaining background. Standard particle identification, based on particle dependent time profile of photon emission in liquid scintillator, can not be used given the identical mass of the two particles. However, the positron annihilation is sometimes delayed by the orthopositronium (o-Ps) metastable state formation, which induces a pulse shape distortion that could be used for positron identification. In this paper we report on the first observation of positronium formation in a large liquid scintillator detector based on pulse shape analysis of single events. The o-Ps formation fraction and its lifetime were measured, finding the values of 44 +/- 12 % (sys.) +/- 5 % (stat.) and 3.68 ns +/- 0.17 ns (sys.) +/- 0.15 ns (stat.) respectively, in agreement with the results obtained with a dedicated positron annihilation lifetime spectroscopy setup.

Journal Of High Energy Physics [10], 032, 2014. DOI: 10.1007/JHEP10(2014)032

[P342-2014] "Paired evaluation of calvarial reconstruction with prototyped titanium implants with and without ceramic coating"

Calderoni, D. R.; Gilioli, R.; Munhoz, A. L. J.; Maciel, R.; Zavaglia, C. A. D.; **Lambert, C. S.***; Lopes, E. S. N.; Toro, I. F. C.; Kharmandayan, P.

PURPOSE: To investigate the osseointegration properties of prototyped implants with tridimensionally interconnected pores made of the Ti6Al4V alloy and the influence of a thin calcium phosphate coating. METHODS: Bilateral critical size calvarial defects were created in thirty Wistar rats and filled with coated and uncoated implants in a randomized fashion. The animals were kept for 15, 45 and 90 days. Implant mechanical integration was evaluated with a push-out test. Bone-implant interface was analyzed using scanning electron microscopy. RESULTS: The maximum force to produce initial displacement of the implants increased during the study period, reaching values around 100N for both types of implants. Intimate contact between bone and implant was present, with progressive bone growth into the pores. No significant differences were seen between coated and uncoated implants. CONCLUSION: Adequate osseointegration can be achieved in calvarial reconstructions using prototyped Ti6Al4V Implants with the described characteristics of surface and porosity.

Acta Cirurgica Brasileira 29[9], 579-587, 2014. DOI: 10.1590/S0102-86502014000150005

[P343-2014] "Performance of the ALICE experiment at the CERN LHC"

Abelev, B.; Abramyan, A.; Adam, J.; **Chinellato, D. D.*; Dash, A.*; Takahashi, J.*;** et al.
ALICE Collaboration

ALICE is the heavy-ion experiment at the CERN Large Hadron Collider. The experiment continuously took data during the first physics campaign of the machine from fall 2009 until early 2013, using proton and lead-ion beams. In this paper we describe the running environment and the data handling procedures, and discuss the performance of the ALICE detectors and analysis methods for various physics observables.

International Journal Of Modern Physics A 29[24], 1430044, 2014. DOI: 10.1142/S0217751X14300440

[P344-2014] "Probing the surface atomic structure of Au/Cr2O3/Pd(111) by photoelectron diffraction"

Kilian, A. S.; Pancotti, A.; **Landers, R.*; de Siervo, A.***; Morais, J.

A detailed investigation concerning the surface atomic structure of the Au/Cr2O3 model catalyst deposited on a Pd(111) single crystal surface is presented. The system was prepared by molecular beam epitaxy (MBE) and characterized in situ by low-energy electron diffraction (LEED), X-ray photoelectron spectroscopy (XPS) and X-ray photoelectron diffraction (XPD). The element-specific short-range order information was obtained from XPD experiments supported by a comprehensive multiple scattering calculation diffraction approach. Based on the experiments, we have strong evidence of Au island formation on the Cr2O3 surface. The experiments indicated that the islands are constructed of two Au monolayers and formed by the important structural relaxations in the three outermost atomic layers of the Au/Cr2O3 surface. Such a surface structure could explain the particular catalytic reactivity displayed by catalysts based on Au nanoparticles dispersed on several oxide matrices.

Crystengcomm 16[39], 9291-9298, 2014. DOI: 10.1039/c4ce01389a

[P345-2014] "Recalibration of U-doped standard glasses through uranium thin film for neutron-fluence measurements"

Soares, C. J.*; Guedes, S.*; Curvo, E. A. C.; **Hadler, J. C.***; Jonckheere, R.; Tello, C. A.; **Lixandro, A. L.*;** Siqueira, P. T. D.; Madi Filho, T.

This work presents a recalibration of U-doped standard glasses using natural uranium thin films to be used as most dedicated neutron monitor for fission-track dating. The recalibrated U-doped glasses were used to determine fission-track ages in apatite samples from Brazilian alkaline formations (Alto Paranaiba) and standard Durango apatite. Samples were irradiated in two nuclear reactors with different characteristics and the results were compared. For well-thermalized neutron facility, metal activation monitor was also used. The ages of Alto Paranaiba arch and Durango apatite agree with those determined by other radiometric dating methods and metal activation monitors. These results suggest that the presented recalibration is suitable to be used routinely for fission-track dating studies even in a non-well thermalized neutron facility.

Journal Of Radioanalytical And Nuclear Chemistry 302[1], 17-26, 2014. DOI: 10.1007/s10967-014-3296-6

[P346-2014] "Reviewing the latest results from the Pierre Auger Observatory"

Dobrigkeit, C.*
Pierre Auger Collaboration

The Pierre Auger Observatory was built to help unveil the properties of ultra-high energy cosmic rays with energies from 10(17) to 10(20) eV. In this paper we review the latest results obtained from data of the Pierre Auger Observatory in almost ten years of continuous operation and summarize what has been learned about the energy spectrum, mass composition, and arrival directions of cosmic rays in that energy range. We also discuss some implications of these results for the full characterization of ultra-high energy cosmic rays and for assembling a consistent description of their origin, propagation, and composition.

Astronomische Nachrichten 335[6-7], SI, 573-580, 2014. DOI: 10.1002/asna.201412075

[P347-2014] "Search for invisible decays of Higgs bosons in the vector boson fusion and associated ZH production modes"

Chatrchyan, S.; Khachatryan, V.; Sirunyan, A. M.; **Chinellato, J.*; Tonelli Manganote, E. J.*;** et al.
CMS Collaboration

A search for invisible decays of Higgs bosons is performed using the vector boson fusion and associated ZH production modes. In the ZH mode, the Z boson is required to decay to a pair of charged leptons or a bb quark pair. The searches use the 8TeV pp collision dataset collected by the CMS detector at the LHC, corresponding to an integrated luminosity of up to 19.7 fb(-1). Certain channels include data from 7TeV collisions corresponding to an integrated luminosity of 4.9 fb(-1).The searches are sensitive to non-standardmodel invisible decays of the recently observed Higgs boson, as well as additional Higgs bosons with similar production modes and large invisible branching fractions. In all channels, the observed data are consistent with the expected standard model backgrounds. Limits are set on the production cross section times invisible branching fraction, as a function of the Higgs boson mass, for the vector boson fusion and ZH production modes. By combining all channels, and assuming standard model Higgs boson cross sections and acceptances, the observed (expected) upper limit on the invisible branching fraction at m(H) = 125GeV is found to be 0.58 (0.44) at 95% confidence level. We interpret this limit in terms of a Higgs-portal model of dark matter interactions.

European Physical Journal C 74[8], 2980, 2014. DOI: 10.1140/epjc/s10052-014-2980-6

[P348-2014] "Searches For Large-Scale Anisotropy In The Arrival Directions Of Cosmic Rays Detected Above Energy Of 10(19) Ev At The Pierre Auger Observatory And The Telescope Array"

Aab, A.; Abreu, P.; Aglietta, M.; **Chinellato, J. A.*; Daniel, B.*; Diaz Castro, M. L.*; Dobrigkeit, C.*; Escobar, C. O.*; Fauth, A. C.*; Muller, M. A.*; Pakk Selmi-Dei, D.*; Santos, E.*; Theodoro, V. M.*; Silva, M. Zimbres***; et al.
Pierre Auger Collaboration; Array Collaboration

Spherical harmonic moments are well-suited for capturing anisotropy at any scale in the flux of cosmic rays. An unambiguous measurement of the full set of spherical harmonic coefficients requires full-sky coverage. This can be achieved by combining data from observatories located in both the northern and southern hemispheres. To this end, a joint analysis using data recorded at the Telescope Array and the Pierre Auger Observatory above 10(19) eV is presented in this work. The resulting multipolar expansion of the flux of cosmic rays allows us to perform a series of anisotropy searches, and in particular to report on the angular power spectrum of cosmic rays above 10(19) eV. No significant deviation from isotropic expectations is found throughout the analyses performed. Upper limits on the amplitudes of the dipole and quadrupole moments are derived as a function of the direction in the sky, varying between 7% and 13% for the dipole and between 7% and 10% for a symmetric quadrupole.

Astrophysical Journal 794[2], 172, 2014. DOI: 10.1088/0004-637X/794/2/172

[P349-2014] "Site specific spin dynamics in BaFe2As2: tuning the ground state by orbital differentiation"

Rosa, P. F. S.*; Adriano, C.*; Garitezi, T. M.*; Grant, T.; Fisk, Z.; **Urbano, R. R.*; Pagliuso, P. G.***

The role of orbital differentiation on the emergence of superconductivity in the Fe-based superconductors remains an open question to the scientific community. In this investigation, we employ a suitable microscopic spin probe technique, namely Electron Spin Resonance (ESR), to investigate this issue on selected chemically substituted BaFe2As2 single crystals. As the spin-density wave (SDW) phase is suppressed, we observe a clear increase of the Fe 3d bands anisotropy along with their localization at the FeAs plane. Such an increase of the planar orbital content is interestingly independent of the chemical substitution responsible for suppressing the SDW phase. As a consequence, the magnetic fluctuations in combination with this particular symmetry of the Fe 3d bands are propitious ingredients for the emergence of superconductivity in this class of materials.

Scientific Reports 4, 6543, 2014. DOI: 10.1038/srep06543

[P350-2014] "Species fractionation in atomic chains from mechanically stretched alloys"

Autreto, P. A. D.*; Galvao, D. S.*; Artacho, E.

Bettini et al (2006 Nat. Nanotechnol. 1 182-5) reported the first experimental realization of linear atomic chains (LACs) composed of different atoms (Au and Ag). The different contents of Au and Ag were observed in the chains from what was found in the bulk alloys, which raises the question of what the wire composition is, if it is in equilibrium with a bulk alloy. In this work we address the thermodynamic driving force for species fractionation in LACs under tension, and we present the density--functional theory results for Ag-Au chain alloys. A pronounced stabilization of the wires with an alternating Ag-Au sequence is observed, which could be behind the experimentally observed Au enrichment in LACs from alloys with high Ag content.

Journal Of Physics-Condensed Matter 26[43], 435304, 2014. DOI: 10.1088/0953-8984/26/43/435304

[P351-2014] "Spectroscopic properties of Er3+-doped sodium-modified tellurite glasses for use as optical amplifiers at 1540 nm"

Rivera, V. A. G.; **Barbosa, L. C.***

The impact of different sodium concentrations on the thermal properties and near-infrared emission at 1540 nm of Er3+-doped tellurite glasses was investigated. The glasses were characterized by UV-visible-near-infrared absorption spectroscopy, emission spectroscopy, Raman spectroscopy, refractive index measurements, and lifetime estimates. A theoretical analysis of the prepared samples was performed with the Judd-Ofelt parameters, radiative transition probability, quantum yield, and radiative lifetime. The glasses presented a large calculated emission cross-section at around 1537 nm (8.4 x 10(-21) cm(2)) and a good quantum yield (93%). The spectroscopic quality factors (Omega(4)/Omega(6)) obtained for the samples showed good agreement with the emission spectrum and bandwidth in the near-infrared region. The advantageous spectroscopic characteristics, together with good thermal stability, indicate that the glasses have potential applications as 1540 nm waveguides.

Journal Of Luminescence 156, 116-123, 2014. DOI: 10.1016/j.jlumin.2014.07.023

[P352-2014] "Study of hadronic event-shape variables in multijet final states in pp collisions at root s=7 TeV"

Khachatryan, V.; Sirunyan, A. M.; Tumasyan, A.; **Chinellato, J.***; et al.
CMS Collaboration

Event-shape variables, which are sensitive to perturbative and nonperturbative aspects of quantum chromodynamic (QCD) interactions, are studied in multijet events recorded in proton-proton collisions at root s = 7 TeV. Events are selected with at least one jet with transverse momentum p(T) > 110 GeV and pseudorapidity vertical bar eta vertical bar < 2.4, in a data sample corresponding to integrated luminosities of up to 5 fb(-1). The distributions of five event-shape variables in various leading jet p(T) ranges are compared to predictions from different QCD Monte Carlo event generators.

Journal Of High Energy Physics [10], 087, 2014. DOI: 10.1007/JHEP10(2014)087

[P353-2014] "The atomic approach for the Coqblin-Schrieffer model"

Figueira, M. S.; Saguia, A.; **Foglio, M. E.*;** Silva-Valencia, J.; Franco, R.

In this work we consider the Coqblin-Schrieffer model when the spin is S=1/2. The atomic solution has eight states: four conduction and two localized states, and we can then calculate the eigenenergies and eigenstates analytically. From this solution, employing the cumulant Green's functions results of the Anderson model, we build a "seed", that works as the input of the atomic approach, developed earlier by some of us. We obtain the T-matrix as well as the conduction Green's function of the model, both for the impurity and the lattice cases. The generalization for other moments within N states follows the same steps. We present results both for the impurity as well as for the lattice case and we indicate possible applications of the method to study ultra cold atoms confined in optical superlattices and Kondo insulators. In this last case, our results support an insulator-metal transition as a function of the temperature.

Physica B-Condensed Matter 455, 92-95, 2014. DOI: 10.1016/j.physb.2014.07.054

[P354-2014] "The atomic structure of a bare buffer layer on SiC(0001) chemically resolved"

de Lima, L. H.*; Handschak, D.; Schonbohm, F.; **Landers, R.*;** Westphal, C.; **de Siervo, A.***

A chemical-specific photoelectron diffraction structure determination of a carbon rich buffer layer on SiC is reported. In addition to the long-range ripple of this surface, a local buckling in the hexagonal sublattice, which breaks the local range order symmetry, was unraveled.

Chemical Communications 50[88], 13571-13574, 2014. DOI: 10.1039/c4cc05005c

Trabalhos Aceitos para Publicação

[A001-2014] "Desenhando, Medindo E Registrando A Temperatura: Aprendendo Ciências E Matemática"

da Paixão, F. J.*

A introdução do ensino de ciências nas séries iniciais tem sido motivada em diversos países seja por documentos oficiais ou por ações da comunidade acadêmica. Entretanto, apesar de haver pesquisas que apontam um grande interesse dos alunos nesta faixa etária, a necessidade de melhorar o aprendizado da língua e da matemática tem levado a ou uma redução do tempo dedicado ao ensino de ciências em alguns locais ou a simples omissão. Pesquisas apontam que atividades investigativas de ciências podem beneficiar o letramento e vice e versa e o mesmo pode ocorrer em relação a matemática. Neste trabalho nós apresentaremos como o ensino de ciências pode levar a melhoria do aprendizado de matemática por numa turma composta por alunos do 2º ano do ensino fundamental numa escola pública. Durante todo o ano os alunos fazem registros de forma individual ou coletivamente, com o objetivo de observar o ano, como visto da terra. As observações compostas por medida da temperatura, desenho do céu, acompanhar a sombra de um objeto e a presença da lua, criavam registos e foram acompanhadas de avaliações mensais dos dados feitas de forma individual e discutidos pequenos grupos. A leitura do termômetro permite adquirir destreza com os números inteiros. O seu tratamento gráfico permite perceber as variações no mês e no ano. A atividade dos desenhos permite os alunos observarem o movimento que o sol faz em relação a terra responsável pelo ano, que também envolve desenvolver uma percepção geométrica. Utilizamos uma análise baseada na construção do conhecimento e em métodos ativos para melhorar o aprendizado em sala de aula.

Aceito para apresentação oral na mesa redonda "A Abordagem Do Ensino De Matemática, De Ciências E Da Avalição Nos Anos Iniciais Do Ensino Básico" no XVII ENDIPE, Fotaleza, Ce, 11-14 de novembro de 2014.

[A002-2014] "Formation energy of graphene oxide structures: a molecular dynamics study on distortion and thermal effects."

Fonseca*, A. F.; Zhang, H.; Kyeongjae Cho.

Ab initio predictions for the stability of different graphene oxide (GO) structures have been shown to conflict with experimental observations. While ab initio studies predict that the most stable GOs are fully oxygen-covered (either with epoxide or hydroxyl), stable as-produced GOs are partially oxygen-covered and predominantly epoxide-covered structures. Although this discrepancy is being examined in terms of calculations of free energies of GOs and large diffusion energy-barriers for oxygen groups on graphene, there is still a lack of understanding on the energetic properties of GOs using classical molecular dynamics, which is able to investigate their structural distortion. Here, using the Reactive Empirical Bond Order (REBO) molecular dynamics potential, we compute the free energy and binding energy of GOs at different oxygen concentrations and epoxide to hydroxyl ratios, as well as the distortion energies of graphene lattice. Although epoxide causes more distortion on the carbon hexagonal planar structure, it provides more stability to the GO structure. The difference between free energy and binding energy of GOs is shown to be independent of oxygen coverage. These results allow gaining more insight on the issue of GO stability and show that REBO can capture most of experimental properties of GOs.

Carbon, Aceito em 5 December 2014. DOI: 10.1016/j.carbon.2014.12.026

Correção

[C077-2014] "Search for the associated production of the Higgs boson with a top-quark pair (vol 9, 087, 2014)"

Khachatryan, V.; Sirunyan, A. M.; Tumasyan, A.; **Chinellato, J.*; Manganote, E. J. Tonelli*;** et al.
CMS Collaboration

Journal Of High Energy Physics [10], 106, 2014. DOI: 10.1007/JHEP10(2014)106

*Autores da comunidade IFGW

Defesas de Dissertações

[D016-2014] "Condensação Bose-Einstein em sistemas de átomos de 4He"
Aluno: Vitor Zamprônio Pedroso
Orientador: Prof. Dr. Silvio Antonio Sachetto Vitiello
Data: 09/12/2014

[D017-2014] "A study on the structure and dynamics of complex networks"
Aluno: João Pinheiro Net
Orientador: Prof. Dr. José Antonio Brum
Data: 15/12/2014

Defesas de Teses

[T026] "Mechanical Properties of HCP 4He"
Aluno: Edgar Josué Landinez Borda
Orientador: Prof. Dr. Maurice de Koning
Data: 01/12/2014

[T027] "Interação entre portadores e íons magnéticos em poços quânticos de InGaAs/GaAs:Mn"
Aluno: Miguel Angel Gonzalez Balanta
Orientador: Profa. Dra. Maria Jose Santos Pompeu Brasil
Data: 04/12/2014

Fonte: Portal IFGW/Pós-graduação - Agenda de Colóquios, Defesas e Seminários.
Disponível em: http://portal.ifi.unicamp.br/pos-graduacao

Acesse o portal Abstracta e faça seu cadastro como leitor, para receber em seu email a notificação de cada novo número publicado:

<http://abstracta.ifi.unicamp.br>

Abstracta

Instituto de Física
Diretor: Prof. Dr. Newton Cesario Frateschi
Diretor Associado: Prof. Dr. Luís Eduardo Evangelista de Araujo
Universidade Estadual de Campinas - UNICAMP
Cidade Universitária Zeferino Vaz
13083-859 - Campinas - SP - Brasil
e-mail: secdir@ifi.unicamp.br

Publicação

Biblioteca do Instituto de Física Gleb Wataghin
http://portal.ifi.unicamp.br/biblioteca

Diretora Técnica: Sandra Maria Carlos Cartaxo
Coordenador da Comissão de Biblioteca: Prof. Dr. André Koch Torres de Assis

Elaboração
Maria Graciele Trevisan (Bibliotecária)
contato: infobif@ifi.unicamp.br